

We are IntechOpen, the world's leading publisher of Open Access books Built by scientists, for scientists

5,600

Open access books available

137,000

International authors and editors

170M

Downloads

Our authors are among the

154

Countries delivered to

TOP 1%

most cited scientists

12.2%

Contributors from top 500 universities



WEB OF SCIENCE™

Selection of our books indexed in the Book Citation Index
in Web of Science™ Core Collection (BKCI)

Interested in publishing with us?
Contact book.department@intechopen.com

Numbers displayed above are based on latest data collected.
For more information visit www.intechopen.com



Modeling Grounding Systems for Electromagnetic Compatibility Analysis

*Antonio Carlos S. Lima, Pedro H.N. Vieira,
Marco Aurélio O. Schroeder and Rodolfo Antônio R. Moura*

Abstract

In recent years, the development of smart grids for power distribution and the increasing usage of 5G communication networks have played a large impact on the resilience and reliability of grounding systems. Unexpected electromagnetic coupling between a communication tower and the one used for the electric power networks may pose a threat to the suitable performance of either system as one must assure that electromagnetic compatibility together with unexpected transient issues is within reasonable parameters. This requires wideband modeling of a grounding system, typically carried out using numerical approaches based on the Method of Moments. This modeling is implied in numerous segments to represent the conductors involved and the numerical solution of a double integral for each one of these segments. The modified nodal formulation used to obtain system voltages and branch currents is first solved in the frequency domain, leading to a heavy computational burden and a time-consuming simulation. This chapter briefly reviews the procedure used to model grounding grids and presents some results to illustrate the typical behavior. Afterward, a more complex system comprising a case of electromagnetic coupling is then analyzed to illustrate the impact of nearby grounding grids.

Keywords: grounding systems, method of moments, frequency domain analysis, transient response, computational methods for electromagnetism

1. Introduction

This chapter focuses on the transient analysis of grounding systems and the impact that the associated responses might have with respect to the electromagnetic compatibility in nearby power apparatuses, installations, and people. It is assumed that the reader is familiar with the electromagnetic field theory in both frequency and time domains and some mathematical tools such as Method of Moments [1] and Numerical Laplace Transform [2–6].

The development of smart grids for electric power distribution and the widespread use of 5G communication networks will demand an accurate, efficient, and resilient grounding system to avoid electromagnetic compatibility issues such as interference or noise in apparatuses due to poor power quality, that is, harmonic distortion in voltages and currents. Furthermore, an injected current due to

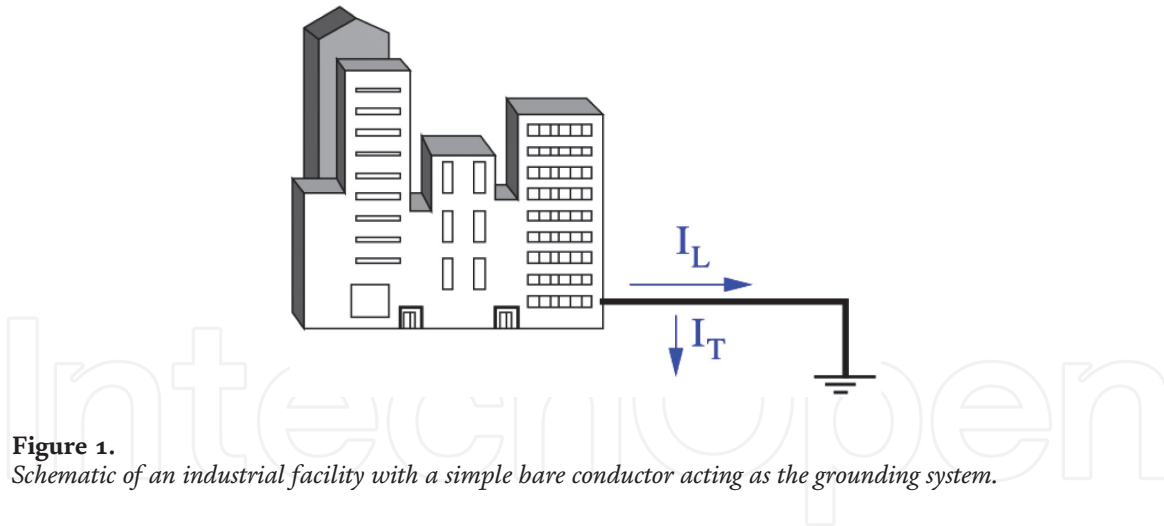


Figure 1.

Schematic of an industrial facility with a simple bare conductor acting as the grounding system.

lightning-related phenomena may lead to a ground potential rise (GPR) that could damage several devices and play an important aspect in the reduction of personal safety in the area surrounding the apparatuses. The most common approach to overcome these possible challenges is to design a feasible, reliable, and efficient grounding system. Therefore, it is of utmost importance to properly understand the transient behavior of a given grounding system in an electrical power or communication installation and its interaction with its surroundings, be it a sensitive electronic device, another grounding system, people, or even the induced voltage at ground level. In general terms, the main function of a grounding system is to provide a pathway with the lowest possible impedance for faulty currents, leading to the least possible voltage increase at the injection point and in its surrounding area. By faulty current, one may consider the one associated with phenomena such as lightning, switching, misoperation, and more recently, the combined harmonic currents related to the presence of power electronic converters in the electric power network.

To illustrate the general idea, consider the schematic presented in **Figure 1**, where a small facility has a rather simple grounding system. It consists of a bare horizontal conductor buried near the ground surface, for example, 0.5 m. The conductor should be long enough that its longitudinal current I_L decays as smoothly as possible, preferably monotonically decreasing, and reaches to zero before reaching the end of the conductor. The bare conductor is open-ended at the far end. The shunt current I_T represents the injected current in the soil, and it is the main contributor to the voltage increase in the surrounding area. Both currents are distributed in nature, and to account for their behavior, one must consider the frequency dependency of conductor and ground. Even in this simple scenario, one needs to divide the conductor into small segments so the Method of Moments can be applied, thus leading to a large order for all the matrices involved. The segmentation of any given conductor to very small segments is also needed for representing the electromagnetic propagation throughout the conductor and surrounding media.

In actual installations, the scenario is even direr as more complex configurations need to be considered. Transmission towers will demand a counterpoise configuration involving an arrangement of conductors that are not parallel for some extension of their lengths. In some scenarios, there are horizontal and vertical conductors to be considered. **Figure 2(a)** depicts the basic structure of a counterpoise for grounding a power transmission tower. Electric power substations demand a grounding grid, which is complex and large in dimensions, representing a challenge for an accurate simulation of transient behavior. **Figure 2(b)** shows a nonuniform grounding grid typically found in electric power substations.

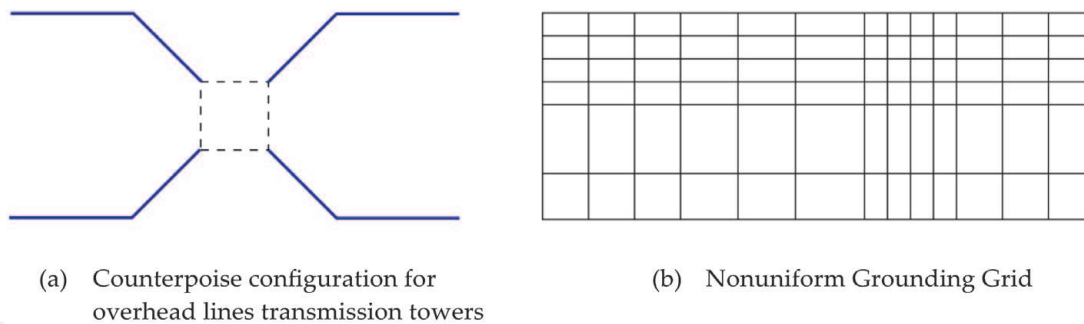


Figure 2. Two grounding grids configuration. (a) Counterpoise configuration for overhead line transmission towers and (b) nonuniform grounding grid.

Although the grounding grid is an element to ensure equipment and people safety, it may have some drawbacks. For instance, an unexpected electromagnetic coupling between a communication tower and the one used for the power network may pose a threat for the suitable performance of electronic equipment as one must assure that electromagnetic compatibility, together with unexpected transient issues, is within reasonable parameters.

In the following sections, we present a mathematical approach based on the Method of Moments to accurately represent a given grounding system. It is a formulation suitable for the analysis related to electromagnetic compatibility issues, as well as the associated current and voltage transient analysis. It is based on the frequency domain formulation of a modified nodal admittance matrix with time responses being obtained using the Numerical Laplace Transform.

2. Mathematical modeling of the equivalent circuit

As commented before, for an accurate assessment of the transient response of the grounding system, a wideband representation is commonly required. The frequency range of lightning-related phenomena goes from a few hertz up to tenths of MHz. Thereby, in the frequency domain, a detailed representation is warranted by using approaches such as the Finite Element Method (FEM) [7] or the Method of Moments (MoM) [8–10]. It is also worth noticing that there are methods that properly solve this numerical issue by solving Maxwell equations directly in the time domain, such as the so-called Finite Differences Time Domain (FDTD) [11, 12]. However, these approaches usually take even more computational time and do not consider the frequency dependence of the soil. In this scenario, considering full-wave frequency domain techniques, there are essentially two approaches to do so. The first one relies on solving Maxwell equations (or the associated vector and scalar potentials) numerically, while the second one applies circuit theory approximation whenever possible. For the latter, there are two approaches in the literature that, although developed independently, share a “common kernel.” The first one is called partial element equivalent circuit (PEEC) [13, 14] and has focused mainly on electromagnetic compatibility issues. The second one is the so-called hybrid electromagnetic model (HEM) [10] and was initially developed to analyze underground bare conductors such as the ones found in electrical grounding. It is important to highlight that the so-called HEM is a particular case of the PEEC in the frequency domain, considering only cylindrical conductors.

Given that both approaches lead to an equivalent circuit derived from the behavior of the electromagnetic fields, these methods can be understood as hybrid models. Regardless of the adopted approach, one needs to divide the conductors

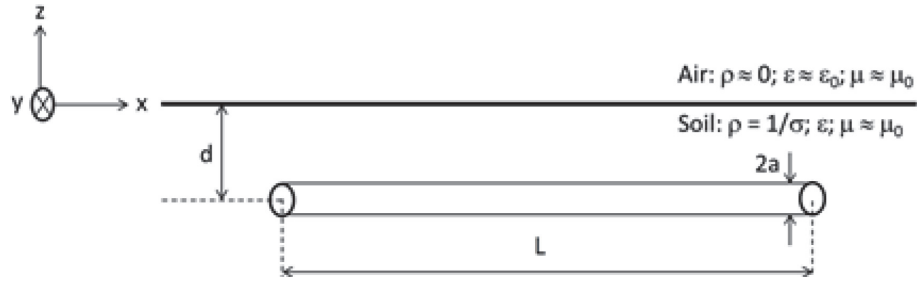


Figure 3.
Horizontal grounding electrode: Real physical system.

involved in several shorter segments to assume a uniform electric current through it and another uniform current, leaving the segment into the surrounding media. Thus, all methods present a heavy computational burden, demanding an improvement of their numerical performance.

In general, hybrid models consist of segmenting the grounding systems into small segments and estimating the electric current that circulates along each segment (here called longitudinal current or I_L) and the current that flows from the electrode to the soil (here called transversal current or I_T). Since these currents are not known previously, it is necessary to apply the MoM to estimate these parameters. To clarify this procedure, consider, as an example, the horizontal grounding electrode shown in **Figure 3**. In this simple case, there are only two semi-infinite media: air and soil. The electrode, with length L , radius a is buried at depth d in a linear, isotropic, and homogeneous soil, with electrical resistivity ρ (electrical conductivity $\sigma = 1/\rho$), electrical permittivity ϵ , and magnetic permeability μ . In general, according to data [15], the magnetic permeability of the soil is close to that of the vacuum ($\mu \approx \mu_0$). The air has $\rho_{\text{air}} \rightarrow \infty$ ($\sigma_{\text{air}} \rightarrow 0$), $\epsilon_{\text{air}} \approx \epsilon_0$, and $\mu_{\text{air}} \approx \mu_0$.

The first step is to divide the electrode into N segments with length $\ell = L/N$ to solve the problem. Then, the electromagnetic coupling is calculated for each pair of elements considering the contribution of both I_T (1) and I_L (2). The numerical values are obtained considering a simplification of the traditional MoM, that is, considering a piecewise pulse base function (more details about this basis function can be found in [16]). At this point, there are two approaches:

- consider the equivalent circuit obtained and solving it either in time or frequency domain
- obtaining a modified nodal analysis (MNA) [17, 18] and solve the system.

$$u_{mn} = \frac{I_{Tn}}{4\pi[\sigma + j\omega\epsilon]L_n L_m} \int_{L_m} \int_{L_n} \frac{e^{-\gamma r}}{r} d\ell_n d\ell_m \quad (1)$$

$$\Delta U_{mn} = -j\omega\mu \frac{I_{Ln}}{4\pi} \int_{L_m} \int_{L_n} \frac{e^{-\gamma r}}{r} d\vec{\ell}_n \cdot d\vec{\ell}_m \quad (2)$$

As in PEEC, HEM considers that both I_T and I_L do not vary along the electrode, i. e., it is uniform for each segment. Since the currents do not vary along the electrode, it is possible to represent a linear system concentrating half of each I_{Tn} in each node that composes a particular segment and considering Kirchhoff Current Law (KCL) in each of these nodes, i. e., considering a pi-equivalent system, similar to the one illustrated in **Figure 4(a)**. Another possibility is to consider a T-equivalent circuit (similar to the one illustrated in **Figure 4b**) and apply the KCL.

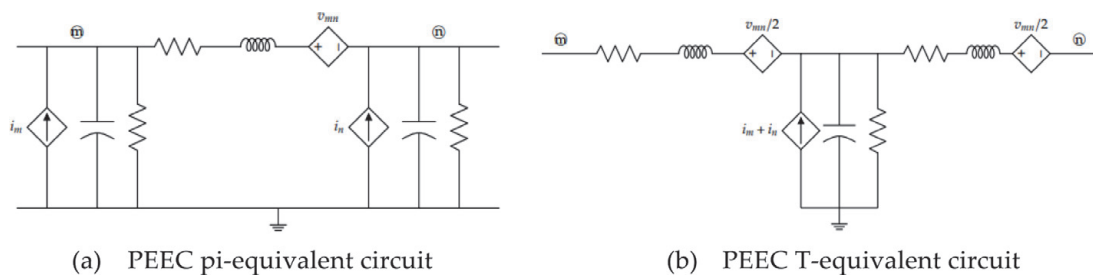


Figure 4. Equivalent circuits obtained to apply the circuit theory in PEEC-type simulation. (a) PEEC pi-equivalent circuit and (b) PEEC T-equivalent circuit.

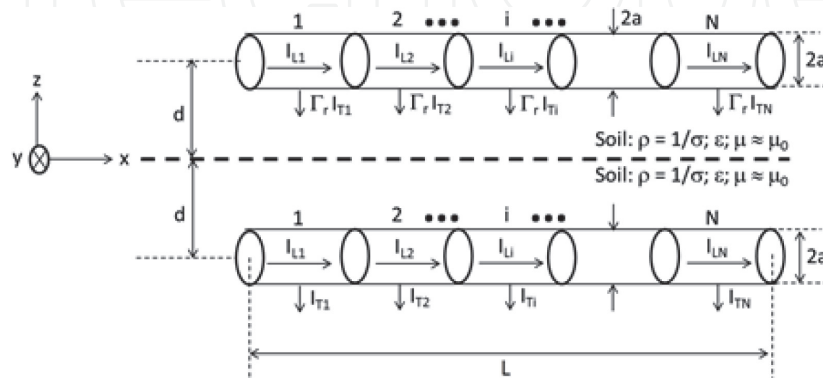


Figure 5. Horizontal grounding electrode: corresponding model.

Furthermore, the interface must be considered. Hence, a classical solution in hybrid models is using the so-called “Image Methods” (IM) [19–21]. **Figure 5** illustrates the equivalent physical system obtained by applying the IM already considering the electrode subdivided into N segments and considering uniform currents in each element.

Additionally, it is important to comment that two main bottlenecks guarantee computational inefficiency:

1. one is related to segmenting the electrode, leading to large and dense matrices;
2. other is associated with a large number of numerical integration of terms in the form of $(e^{-\gamma r}/r)$, leading to a high time-consuming process.

Moreover, these two computationally intense tasks are to be performed at every frequency sample. To overcome such problems, there are some technical propositions in the literature. In [22], the possibility of increasing each segment length is discussed to reduce the matrices’ size, leading to a reduction in the computational burden. In [23], it is presented an alternative to the problem by presenting an average exponential term, that is, approximating the $(e^{-\gamma r}/r)$ as an average value along the electrode, this leads to the necessity of solving the numerical integral only once for each segment. In [24, 25], it is proposed to use the first term in the MacLaurin series expansion of the integrand to obtain a closed form approximation. Since it is necessary to solve the system just once in both cases, it reduces the computational time. Note that these approximations have presented a feasible alternative in most cases (considering that the inject current has a limit frequency band below the 10 MHz). If the frequency spectrum is superior to 10 MHz, these approximations should be avoided. The Appendix presents a relationship between electromagnetic fields and more practical parameters (potential difference, voltage

drop, and step voltage). If the reader is not familiar with the potential/voltage concepts, the authors recommend that the reader goes to the Appendix.

3. Case studies and results

Some case studies were selected to show the response in both frequency and time domains. For the frequency domain analysis, harmonic analysis is performed by injecting a 1A current in every frequency. In the time domain, a double exponential function with unit amplitude was injected to simulate a 0.1/50 μs wave, illustrated in **Figure 6** and given by (3), in *A*. The investigated quantities are the harmonic impedance, GPR, and step voltage along a 1 – m straight line in the $+x$ -direction, calculated both by the potential difference Δu and by the voltage drop U_{p1-p2} , as defined in the Appendix. Note: the $-z$ -direction is the one considered downward, that is, deeper in the soil.

$$i(t) = e^{-2 \times 10^4 t} - e^{-10^7 t} \quad (3)$$

3.1 Horizontal electrode

The first investigation is of a horizontal electrode, 15 m long with a 7 mm radius. The conductor starts at $x = 2.5$ m and ends at $x = 17.5$ m. A current of 1A is injected in the $x = 2.5$ m point of the conductor. Two cases are considered: a soil which low-frequency conductivity σ_0 is 1 mS and other which it is 10 mS. In both cases, the Alipio-Visacro soil model is used with mean values [26].

This case is very similar to the one presented by Alipio et al. [27] but has an important difference: The soil models used therein were both with constant parameters and one presented by Portela et al. [28]. Therefore, a difference in their results is expected because the Portela soil model overestimates the soil conductivity in higher frequencies compared to the Alipio-Visacro soil model used here.

The harmonic impedance is shown in **Figure 7**. According to these results, in the low-frequency spectrum, it is mainly resistive, thus being approximately modeled by a resistor. However, up to a few megahertz, its capacitive and inductive

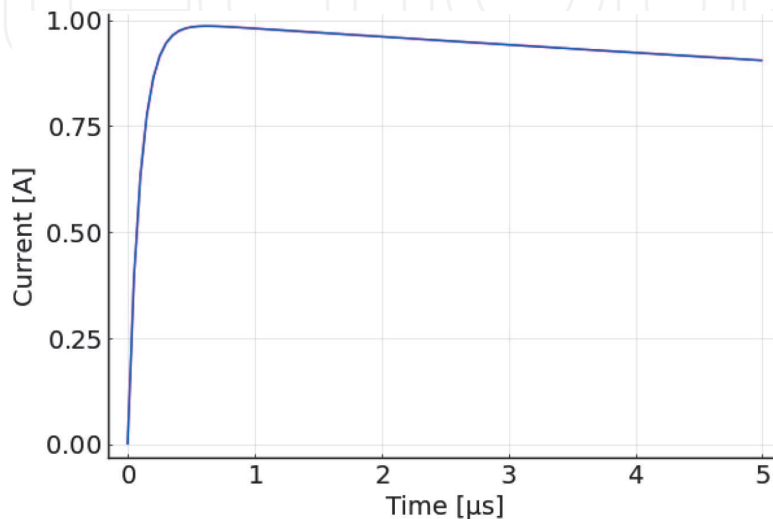


Figure 6.
Injected current for time-domain analysis.

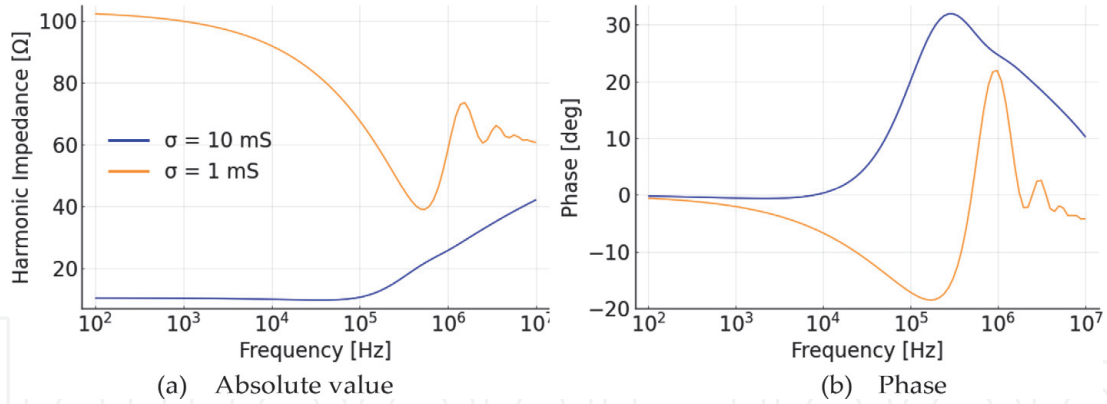


Figure 7. Harmonic impedance of a horizontal electrode. (a) Absolute value and (b) phase.

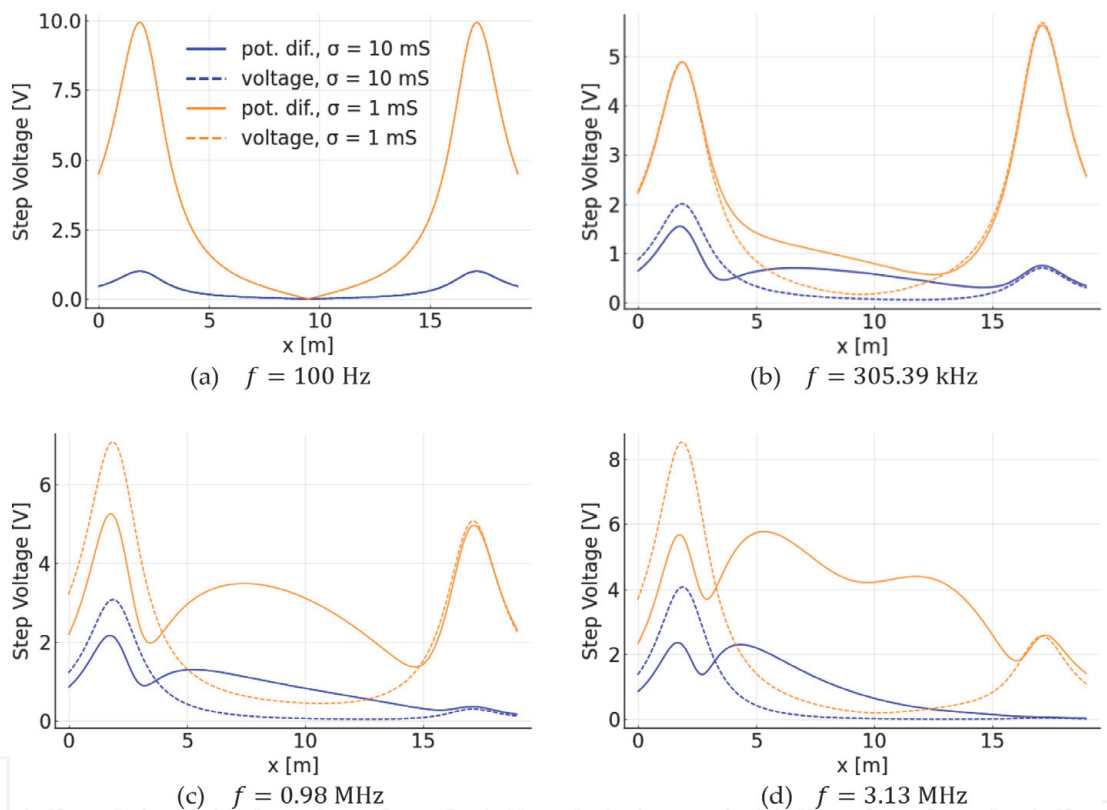


Figure 8. Harmonic step voltage above a horizontal electrode comparing the potential difference Δu and voltage drop U_{p1-p2} . (a) $f = 100$ Hz, (b) $f = 305.39$ kHz, (c) $f = 0.98$ MHz, and (d) $f = 3.13$ MHz.

natures start to play an important role. These pieces of information can be seen in both module and phase values. This impact is even more pronounced in low conductivity soil.

The harmonic step voltage absolute value is shown in **Figure 8**. In low frequencies, the potential difference Δu coincides with the voltage drop U_{p1-p2} . Then, after a few kHz, they begin to differ significantly. This difference is accentuated in higher frequencies. Hence, it is important to consider the nonconservative component of the electric field for high-frequency phenomena.

The GPR is greater for low conductivity soils for the time-domain simulation, as shown in **Figure 9**.

The transient step voltage, illustrated in **Figure 10**, shows a difference between the potential difference Δu and the voltage drop U_{p1-p2} , which is greater in the first

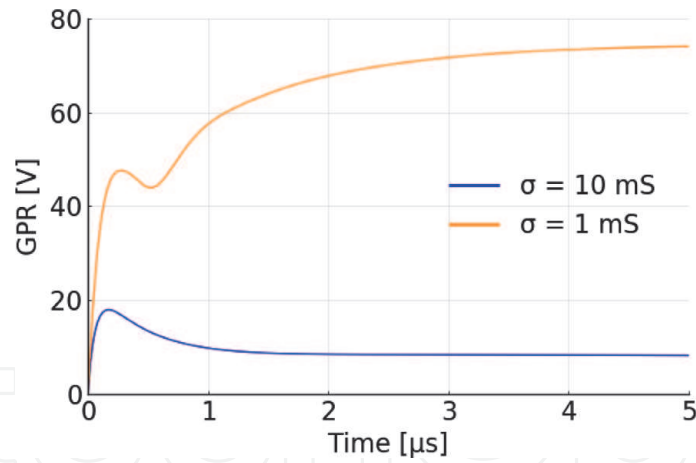


Figure 9.
GPR of a horizontal electrode.

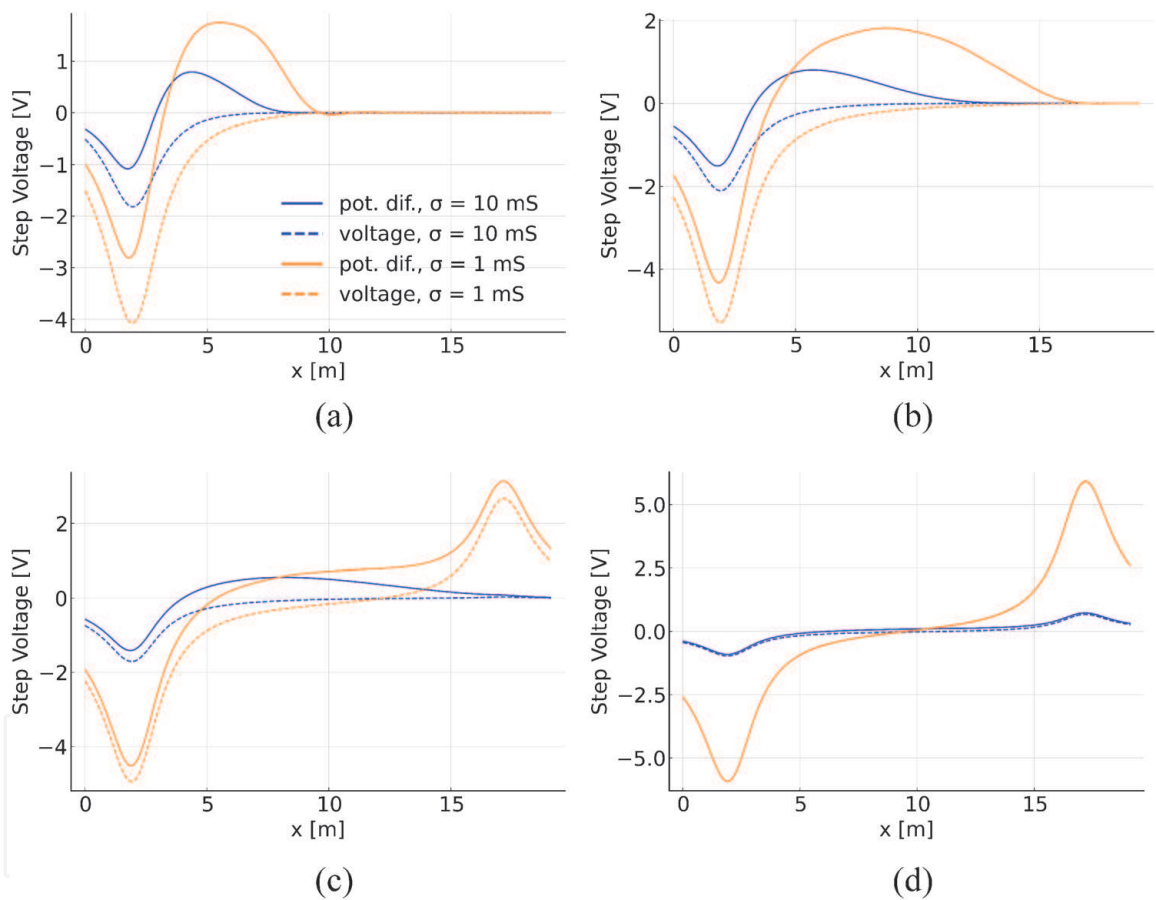


Figure 10.
Transient step voltage above a horizontal electrode comparing the potential difference Δu and voltage drop U_{p1-p2} . (a) $t = 0.1 \mu s$, (b) $t = 0.2 \mu s$, (c) $t = 0.4 \mu s$ and (d) $t = 1.2 \mu s$.

time steps. This difference diminishes when the high-frequency components of the injected current go to zero in later time steps.

3.2 Vertical rod

Another simple case that was investigated is of a vertical rod, but its harmonic impedance and GPR are very similar to that of a horizontal electrode. Moreover, because the longitudinal current is downward in the $-z$ -direction, the

nonconservative electric field only has a component in the z -direction. Therefore, the potential difference Δu is equal to the voltage drop U_{p1-p2} , independently of the frequency. Hence, this case is omitted.

3.3 Rectangular grid

A rectangular grounding grid was investigated, illustrated in **Figure 11**. It is a $20 \times 16 \text{ m}^2$ grid divided into $4 \times 4 \text{ m}^2$ squares buried 0.5 m deep in the soil. It is the same geometric configuration as the one presented in [29], but the soil parameters used here are different. Similarly, to the previous section, the Alipio-Visacro soil model is used with mean values [26] considering, in one case, a low-frequency conductivity σ_0 of 1 mS and 10 mS for the other one.

For this case, the step voltage was calculated in the $+x$ -direction along the line $y = 8$, that is, along the middle of the grid. The current was injected in the grid's corner at $x = y = 0$.

The harmonic impedance of that grid is shown in **Figure 12**. Because the total conductor area is bigger and goes further from the injection point, the harmonic impedance of the grid is smaller than the horizontal electrode. This effect is stronger

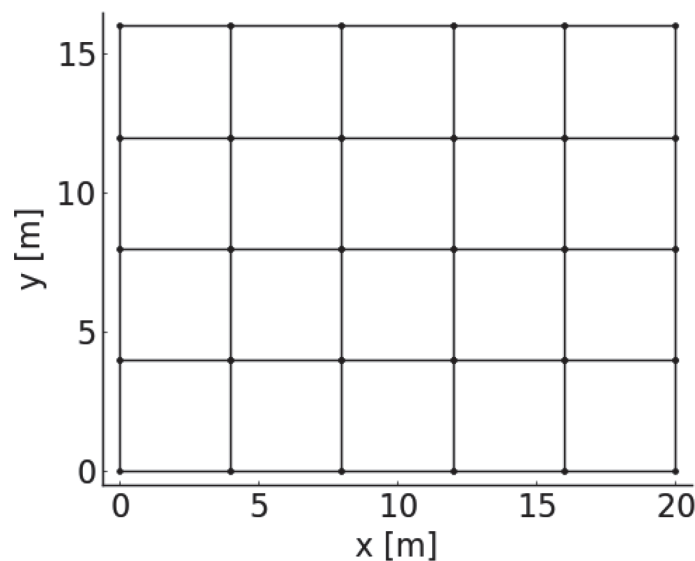


Figure 11.
 Simulated grounding grid.

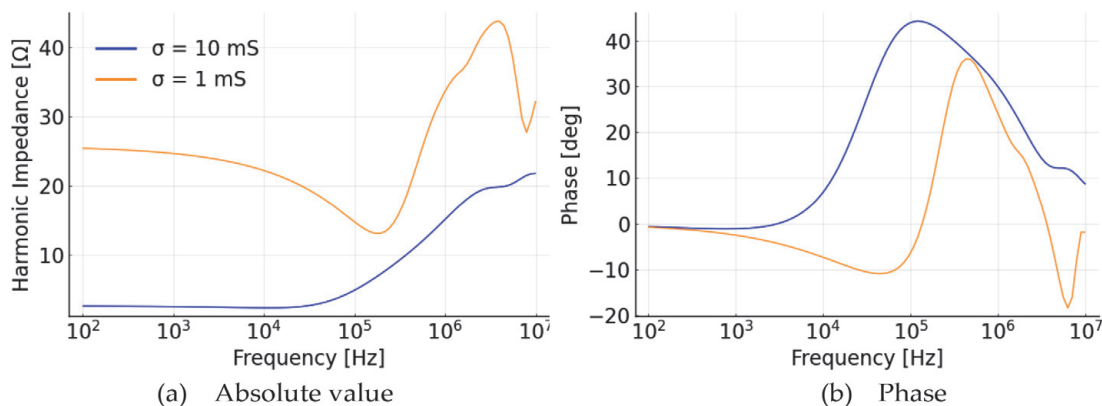


Figure 12.
 Harmonic impedance of a grounding grid. (a) Absolute value and (b) phase.

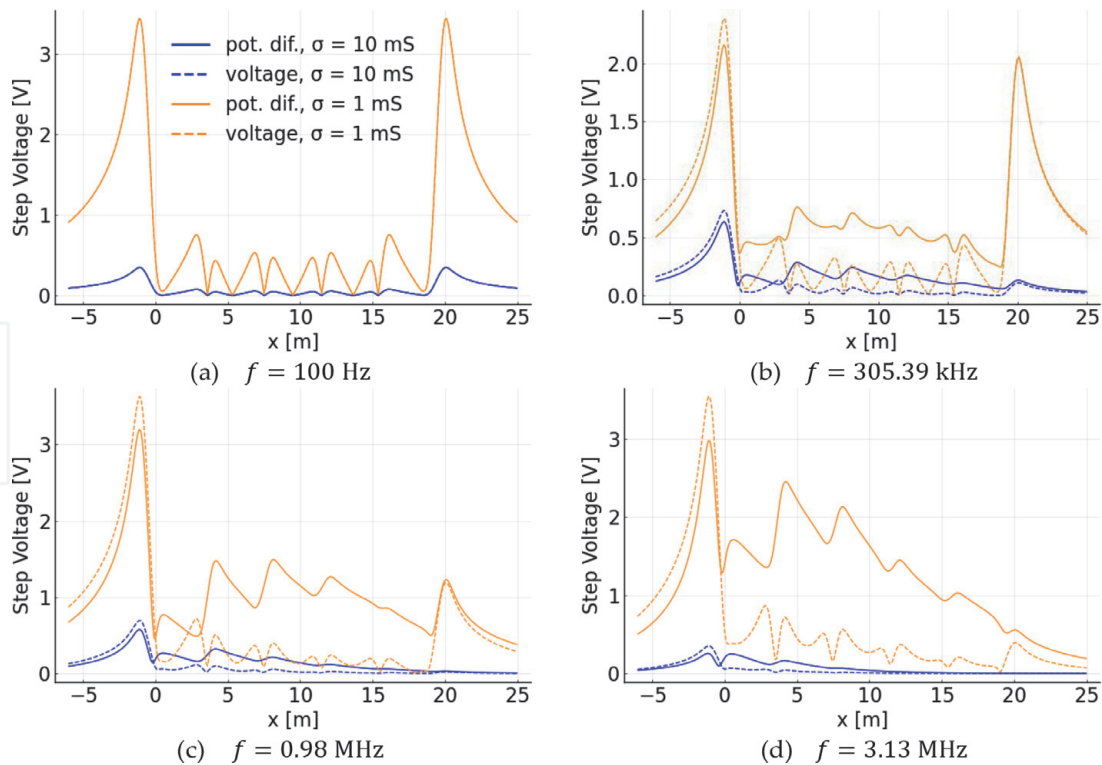


Figure 13.

Harmonic step voltage above a grounding grid comparing the potential difference Δu and voltage drop U_{p1-p2} . (a) $f = 100$ Hz, (b) $f = 305.39$ kHz, (c) $f = 0.98$ MHz, and (d) $f = 3.13$ MHz.

for less conductive soil. The phase behavior of the impedance, however, is very similar.

The harmonic step voltage is shown in **Figure 13**. For low frequencies, the maxima are near the grid edges and peaks when crossing conductors (namely at $x = 0, 4, 8, 12, 16, 20$). Nearer the injection point, the voltage drop U_{p1-p2} is greater than the potential difference Δu . The voltage drop quickly becomes smaller than the potential difference further away from the injection point. The step voltage in a higher conductivity soil is much smaller than that for a low conductivity soil.

The GPR, illustrated in **Figure 14**, is smaller than the one observed for the horizontal conductor due to the smaller harmonic impedance.

The transient step voltage is illustrated in **Figure 15**. There is little coincidence between the potential difference Δu and voltage drop U_{p1-p2} . However, the difference between these quantities takes longer to fade for the grid. The voltage drop has

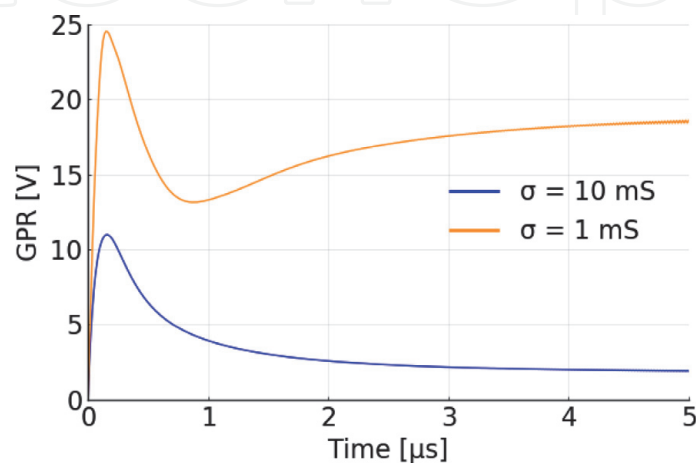


Figure 14.

Ground potential rise (GPR) of a grounding grid.

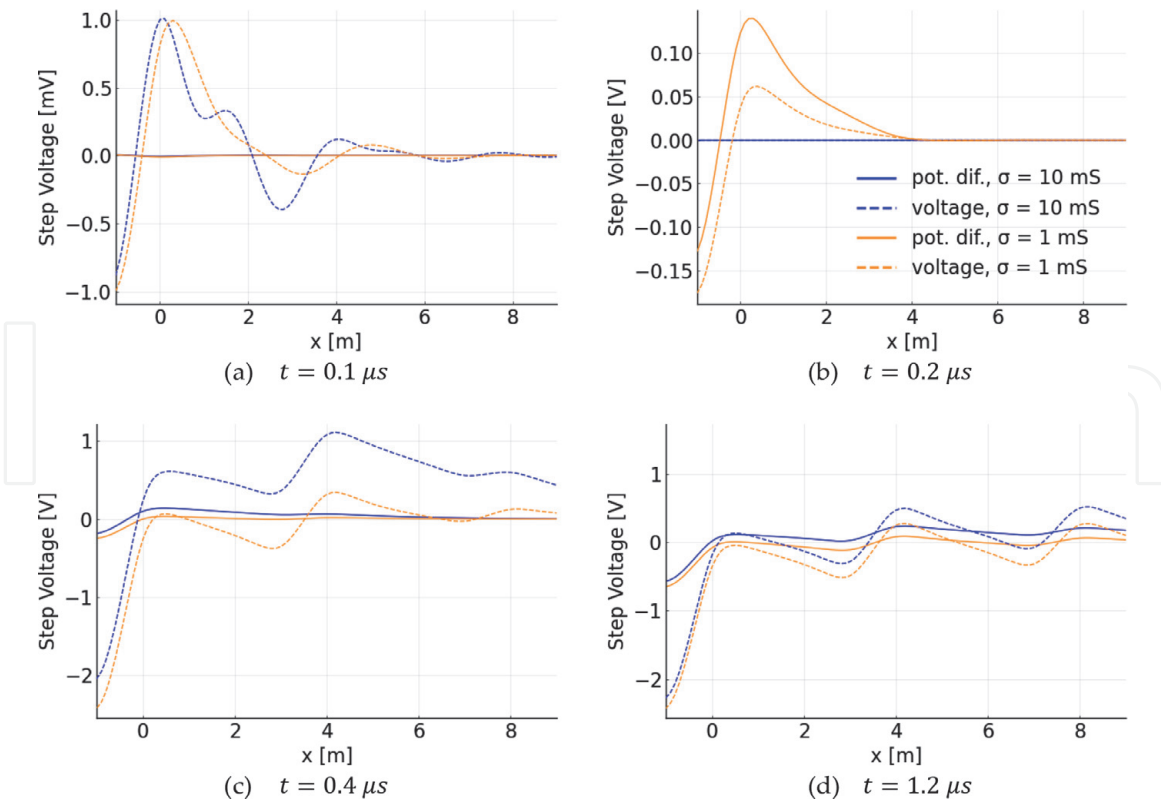


Figure 15. Transient step voltage above a grounding grid comparing the potential difference Δu and voltage drop U_{p1-p2} . (a) $t = 0.1 \mu s$, (b) $t = 0.2 \mu s$, (c) $t = 0.4 \mu s$, and (d) $t = 1.2 \mu s$.

a negative offset due to the nonconservative electric field's direction associated with the conductors' longitudinal currents.

3.4 Three communication towers

This case is about three communication towers in close proximity to each other. All of them are grounded by $12 \times 12 \text{ m}^2$ square grids buried 0.5 m deep. Each grounding grid is 6 m apart from the next one, as illustrated in **Figure 16**. Four cases are considered: having all the grids connected or isolated from each other while the soil is represented by the Alipio-Visacro model [29] with mean values and low-frequency conductivity σ_0 of 1 mS and 10 mS. The current is always injected at the first grid's lower-left corner (the grids are enumerated 1 to 3, from left to right). These connections are a common practice since it reduces the global grounding impedance for low-frequency phenomena.

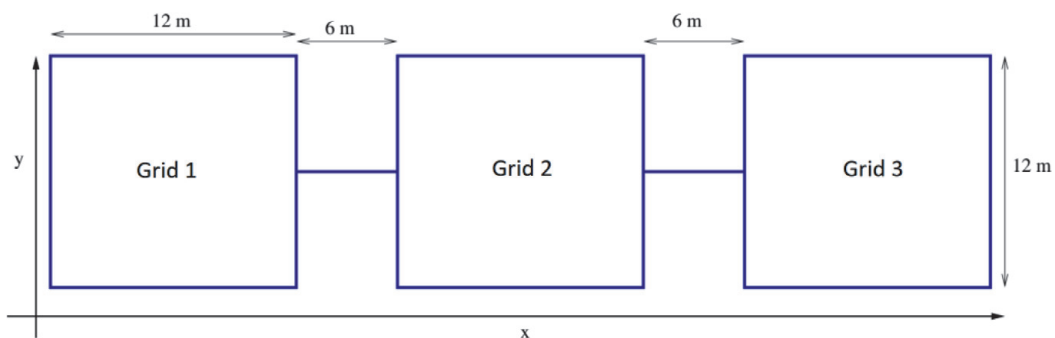


Figure 16. Grounding grids from the communication towers.

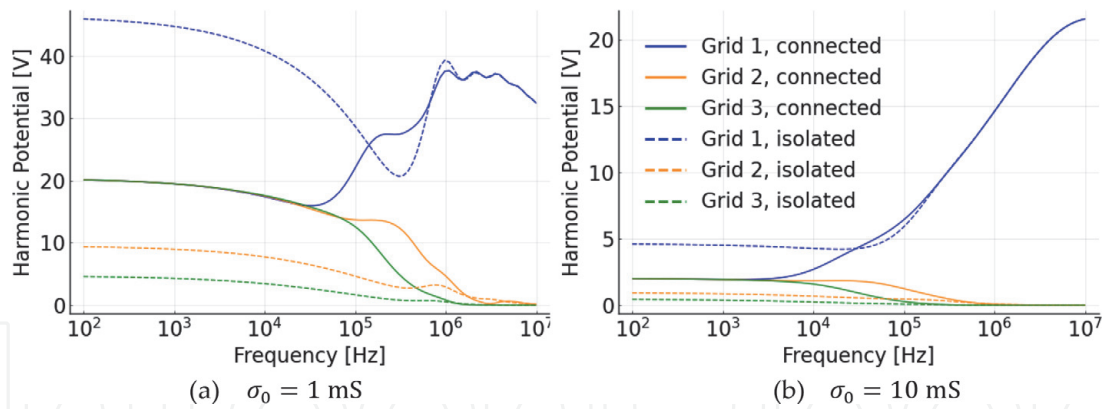


Figure 17. Harmonic potential at the lower-left corner of each tower's grounding grid. (a) $\sigma_0 = 1 \text{ mS}$ and (b) $\sigma_0 = 10 \text{ mS}$.

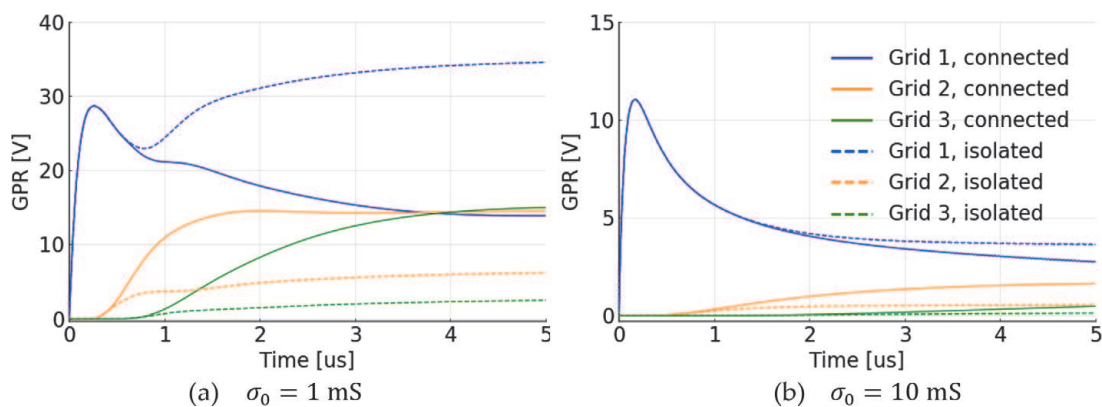


Figure 18. GPR at the lower-left corner of each tower's grounding grids. (a) $\sigma_0 = 1 \text{ mS}$ and (b) $\sigma_0 = 10 \text{ mS}$.

The absolute values of the harmonic potentials that appear at the corner of each grid are shown in **Figure 17**. Connecting the grounding grids of the towers has the effect of equalizing their potentials in low frequencies, reducing the potential that arises in the tower that injects the current in the ground, but raising the potential in the other ones. However, after a few MHz, connecting has practically no effect in reducing harmonic potential. This can be explained based on electromagnetic wave theory. With the increase in both frequency and conductivity, the propagation constant has a greater attenuation constant (real part of the propagation constant). Hence, the nearby grounding grids do not guarantee an actual impact on the potential.

These results show that there is an effective length¹ of the conductors, indicating that for some current excitation, the interconnection between grids does not reduce GPR. Thus, adding more or longer conductors to reduce potential has no practical impact in high frequencies and high conductivity soils, although it is very beneficial

¹ The current dispersed to the soil along the grounding electrode shows nonuniform distribution. This nonuniformity is more pronounced at high frequencies. In this case, the attenuation effects are intense. Associated with this attenuation there is a critical electrode length, such that if a longer electrode is considered there will be no additional current dispersion. At this critical length is given the name of effective length, which depends on the soil conductivity and the frequency spectrum of the injected current.

(and extensively used in grounding design) in steady-state operations. In time-domain analysis, it is possible to notice this phenomenon in the first-time steps. Take **Figure 18(a)**, for instance. Considering Grid 1, until around $0.5 \mu\text{s}$, the curves associated with the connected system and the isolated one are overlapped. However, after that point, the values start to drift away from each other. This is less pronounced in higher conductivity media; see **Figure 18(b)**, for instance.

As mentioned before, connecting the grids has the downside of raising the GPR in the other grids as all of them become equipotential. Thus, it is of utmost importance to properly design the grounding grid, taking into account the equipment that will be connected in these grids as well as the possibility of protecting such elements from unexpected transferred potential. For example, consider **Figure 18(a)**. If a fast current strikes Grid 1 and Grid 2 has sensible electronics equipment connected to it, the potential rise on this equipment will be around three times higher if the grids are connected, leading to a faulted equipment.

As expected from the analysis of previous cases, the harmonic step voltage in the $+x$ -direction calculated by scalar potential difference Δu and calculated by voltage drop U_{p1-p2} has the same numerical values for low frequencies but differ in higher frequencies, as illustrated in **Figures 19** and **20**. That difference is greater when the grids are connected because the current can then travel farther from its injection point and, therefore, cause a stronger electric field above the other grids.

The transient step voltage in the $+x$ -direction is shown in **Figures 21** and **22**. In the first moments, while the injection current is rising, the step voltage has high-frequency components, and the step voltage is zero, far from the first grid.

The step voltage calculated by the voltage drop U_{p1-p2} has a negative offset compared to the potential difference Δu because of the current direction in the conductors, particularly in the conductors that connect the grids. The

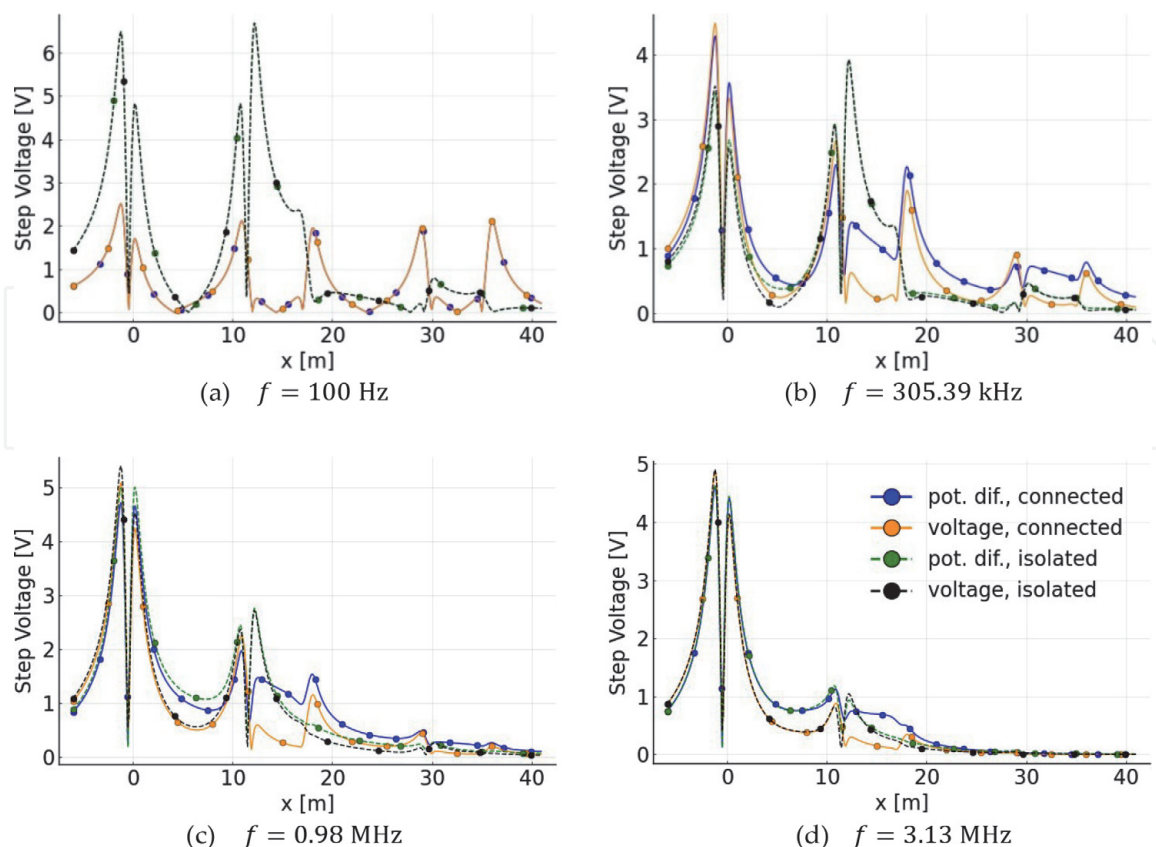


Figure 19. Harmonic step voltage on the ground surface along the line $y = 6 \text{ m}$ comparing the potential difference Δu and voltage drop U_{p1-p2} above the tower's grounding grids for soil with $\sigma_o = 1 \text{ mS}$. (a) $f = 100 \text{ Hz}$, (b) $f = 305.39 \text{ kHz}$, (c) $f = 0.98 \text{ MHz}$, and (d) $f = 3.13 \text{ MHz}$.

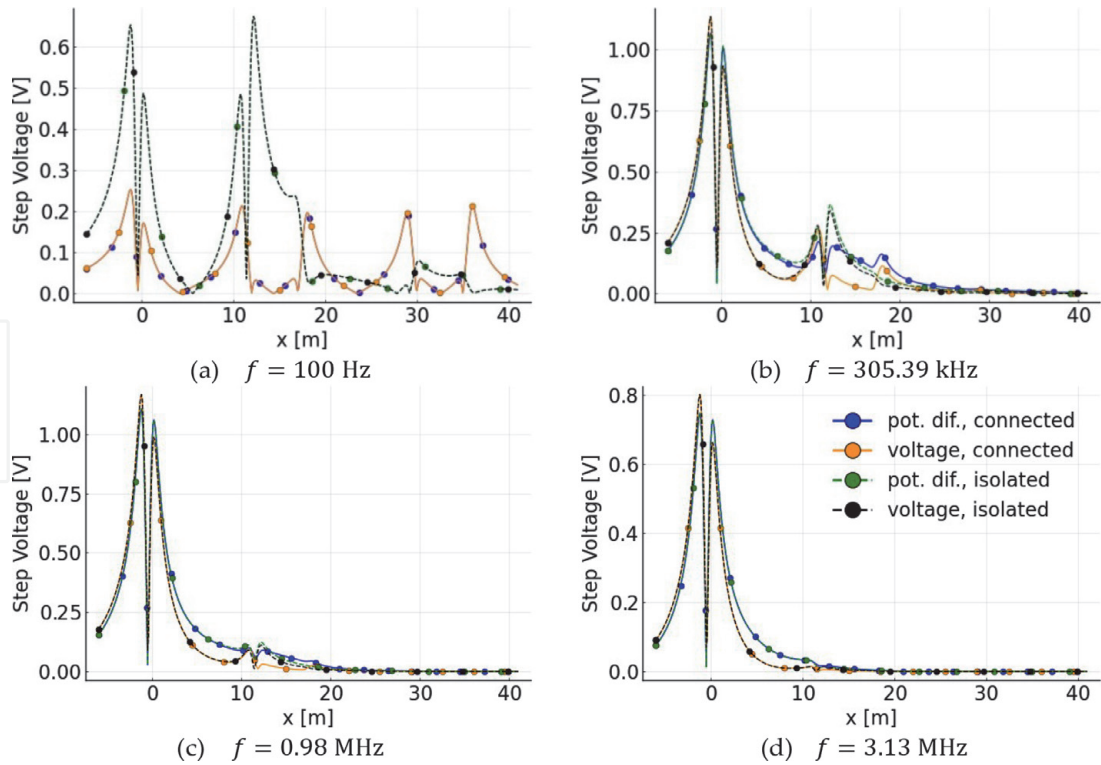


Figure 20. Harmonic step voltage on the ground surface along the line $y = 6 \text{ m}$ comparing the potential difference Δu and voltage drop U_{p1-p2} above the tower's grounding grids for soil with $\sigma_o = 10 \text{ mS}$. (a) $f = 100 \text{ Hz}$, (b) $f = 305.39 \text{ kHz}$, (c) $f = 0.98 \text{ MHz}$, and (d) $f = 3.13 \text{ MHz}$.

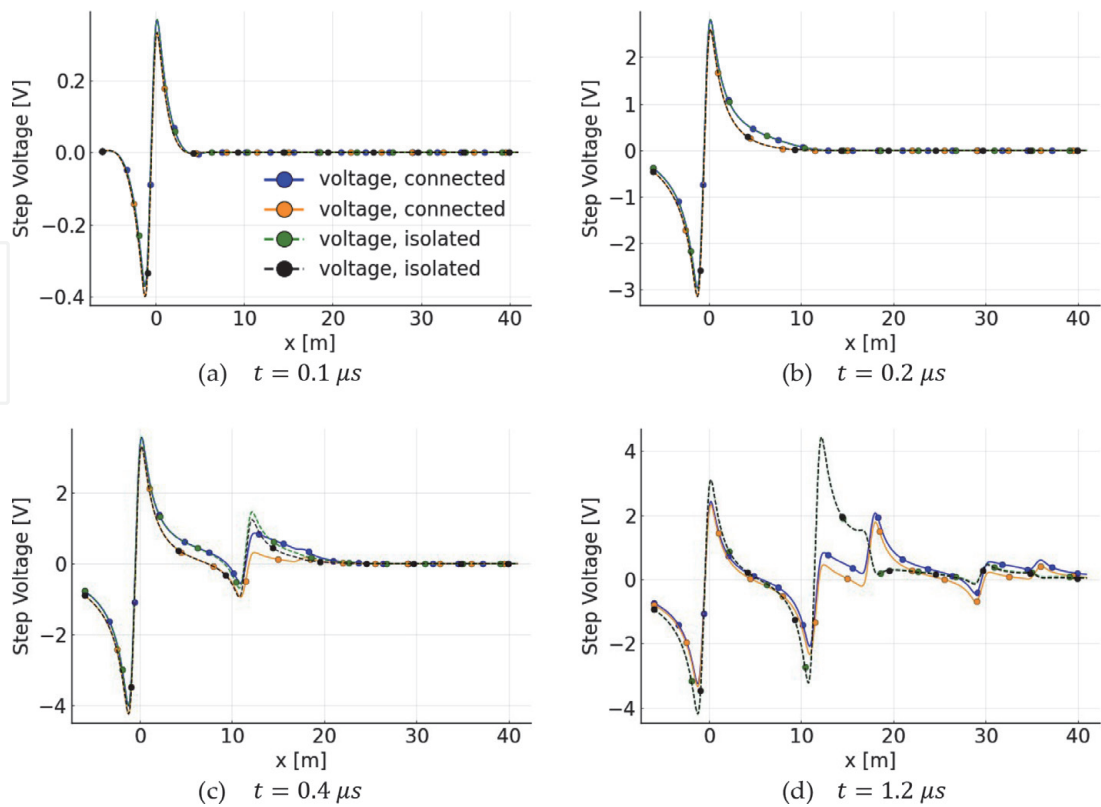


Figure 21. Transient step voltage on the ground surface along the line $y = 6 \text{ m}$ comparing the potential difference Δu and voltage drop U_{p1-p2} above the tower's grounding grids for soil with $\sigma_o = 1 \text{ mS}$. (a) $t = 0.1 \mu\text{s}$, (b) $t = 0.2 \mu\text{s}$, (c) $t = 0.4 \mu\text{s}$, and (d) $t = 1.2 \mu\text{s}$.

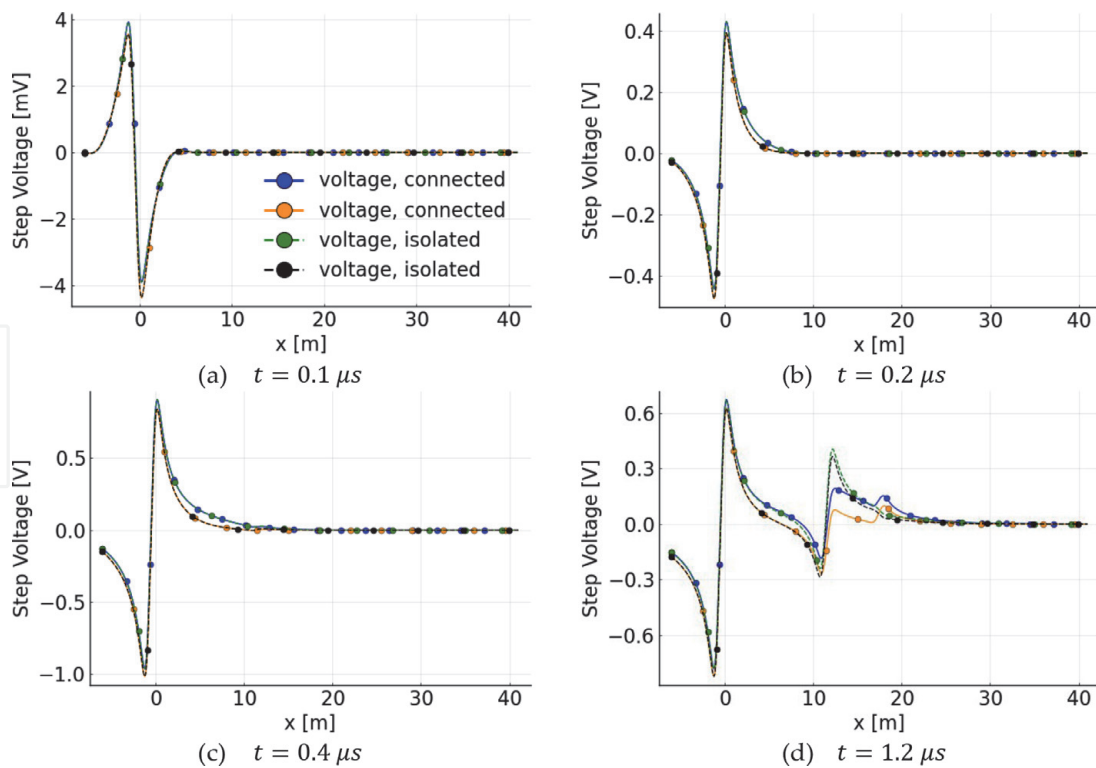


Figure 22. Transient step voltage on the ground surface along the line $y = 6 \text{ m}$ comparing the potential difference Δu and voltage drop $U_{p_1-p_2}$ above the tower's grounding grids for soil with $\sigma_o = 10 \text{ mS}$. (a) $t = 0.1 \mu\text{s}$, (b) $t = 0.2 \mu\text{s}$, (c) $t = 0.4 \mu\text{s}$, and (d) $t = 1.2 \mu\text{s}$.

nonconservative component of the electric field from the currents in the conductors that connect the grids has a $-x$ -direction.

4. Discussions and conclusions

When making an analysis or project, it is essential to be aware of the used mathematical model's simplifications (and limitations thereof). It is often desirable to reduce computational times, usually through mathematical approximations, which restrains the model's applicability. For instance, the results and modeling are presented here to consider all conductors as thin wires.

One approximation that is often made in electromagnetic compatibility and grounding projects is to consider voltage drop (integral effect of the electric field along a given path) as equal to the scalar electric potential difference. However, this will only be true for low-frequency phenomena. As it was shown as an example in the previous sections, the step voltage calculated by integrating the total electric field is different from the scalar potential difference (i.e., considering only the conservative component of the field).

Simplifying the voltage calculation along a path by computing only the scalar potential difference is desirable because that significantly reduces computational time. Unfortunately, that simplification cannot be made except for some low-frequency phenomena. The simulations presented here demonstrate that the voltage drop can be higher or lower than the electric potential difference, depending on the studied case. Hence, more careful approach should be made when calculating the voltage due to lightning, and the total electric field should be integrated.

A common practice is to connect multiple grounding structures that are close to each other. However, the results have shown that connecting multiple grounding structures may not always be beneficial, depending on the intention. In low conductivity soils, that connection has the advantage of reducing the ground potential rise (GPR) of a structure when it is subject to current discharges, but it inadvertently raises the GPR in the other structures. It also has the consequence of raising the step voltage near those other grounding structures. Therefore, the common practices and standard recommendations should be inquired if they are the best for a given project and intention.

A. Appendix: Electromagnetic modeling for determining potential difference, voltage drop, and step voltage

After determining the current distributions in the grounding electrodes, as presented in Section 2, it is possible to calculate the total electric field, the potential difference, and voltage drop. This Appendix presents a brief quantification of these quantities.

A.1 Total electric field \vec{E}_{Total} and its components

Knowing I_T and I_L , it is possible to calculate the total electric field (\vec{E}_{Total}) at a generic point in soil, as well as its conservative (\vec{E}_C) and nonconservative (\vec{E}_{NC}) components. Here, it is called conservative electric field component, the part associated with the transversal current, that is, the one that contemplates the electromagnetic field's divergence nature. On the other hand, here it is called nonconservative electric field component, the part associated with the longitudinal current, that is, the one that contemplates the curling nature of the electromagnetic field.

A.1.1 Conservative electric field component (\vec{E}_C)

To illustrate, consider a point current source I_{T-p} , located in the soil. This current generates an electric scalar potential V_P given by:

$$V_P = \frac{I_{T-p}}{4\pi[\sigma + j\omega\epsilon]} \frac{e^{-\gamma r}}{r} \quad (4)$$

where r is the distance between the source point and the observation point P .

The electric field associated with this current source (\vec{E}_C) is straightforwardly obtained (at any generic point P , into the ground) by the gradient of V_P [27]:

$$\vec{E}_C = -\vec{\nabla}V_P = \frac{I_{T-p}}{4\pi[\sigma + j\omega\epsilon]} \frac{(1 + \gamma r) e^{-\gamma r}}{r^2} \vec{a}_e \quad (5)$$

where \vec{a}_e is the unit vector that defines the direction of \vec{E}_C .

The electric field generated by the total transverse current I_T from a given segment of length $\ell = L/N$ (see **Figure 5**) can be determined by the cumulative effect of point current sources along the segment, considering a continuous and

uniform current distribution with linear density I_{Ti}/L_i . Then, the electric field \vec{E}_{Ci} due to these currents is given by [27]:

$$\vec{E}_{Ci} = \frac{1}{4\pi[\sigma + j\omega\epsilon]} \int_{\ell_i} \frac{I_{Ti} (1 + \gamma r_i) e^{-\gamma r_i}}{L_i r_i^2} d\ell_i \vec{a}_e \quad (6)$$

where r_i is the distance between the infinitesimal element $d\ell_i$ and point P ; \vec{a}_{ei} is the unit vector that defines the direction of \vec{E}_{Ci} .

With similar reasoning, it is possible to determine the conservative electric field component associated with the transverse current of the image segment $\vec{E}_{Ci-image}$.

$$\vec{E}_{Ci-image} = \frac{1}{4\pi[\sigma + j\omega\epsilon]} \int_{\ell_i} \frac{\Gamma_r I_{Ti} (1 + \gamma r_{i-image}) e^{-\gamma r_{i-image}}}{L_i r_{i-image}^2} d\ell_{i-image} \vec{a}_{e-image} \quad (7)$$

where $r_{i-image}$ is the distance between the in the infinitesimal element $d\ell_{i-image}$ and point P ; $\vec{a}_{e-image}$ is the unit vector that defines the direction of $\vec{E}_{Ci-image}$ and Γ_r is the reflection coefficient given by [19, 20] (see **Figure 5**):

$$\Gamma_r = \frac{\sigma + j\omega(\epsilon - \epsilon_0)}{\sigma + j\omega(\epsilon + \epsilon_0)} \quad (8)$$

By considering the system linear and applying the superposition theorem, one can determine the total conservative component $\vec{E}_{Ci-Total}$ associated with the segment i (see **Figure 5**):

$$\vec{E}_{Ci-Total} = \vec{E}_{Ci} + \vec{E}_{Ci-image} \quad (9)$$

Finally, the total conservative component $\vec{E}_{C-Total}$ is obtained *via* the sum of all the conservative field components associated with the transverse currents in the N segments:

$$\vec{E}_{C-Total} = \sum_{i=1}^N (\vec{E}_{Ci} + \vec{E}_{Ci-image}) \quad (10)$$

A.1.2 Nonconservative electric field component (\vec{E}_{NC})

Consider the longitudinal current I_{Li} flowing along segment i (see **Figure 5**). This current source generates a magnetic vector potential \vec{A}_{Pi} at a generic point P of the medium given by:

$$\vec{A}_{Pi} = \frac{\mu_0}{4\pi} \int_{\ell_i} I_{Li} \frac{e^{-\gamma r_i}}{r_i} d\vec{\ell}_i \quad (11)$$

where: $d\vec{\ell}_i$ is the length vector element of segment i , which defines the direction of \vec{A}_{Pi} .

In the frequency domain, the associated nonconservative electric field \vec{E}_{NCi} is given by [27]:

$$\vec{E}_{NCi} = -j\omega\vec{A}_{Pi} = -j\omega\frac{\mu_0}{4\pi}\int_{\ell_i}\frac{e^{-\gamma r_i}}{r_i}d\vec{\ell}_i \quad (12)$$

Similarly, the component corresponding to the image segments $\vec{E}_{NCi\text{-image}}$ is given by [27]:

$$\vec{E}_{NCi\text{-image}} = -j\omega\vec{A}_{Pi\text{-image}} = -j\omega\frac{\mu_0}{4\pi}\int_{\ell_i}\frac{e^{-\gamma r_{i\text{-image}}}}{r_{i\text{-image}}}d\vec{\ell}_{i\text{-image}} \quad (13)$$

In this case, the image method is applied as shown in [21], where the reflection coefficient is equal to the unit, that is, $\Gamma_r = 1$.

Finally, for the total nonconservative component of the electric field $\vec{E}_{NC\text{-Total}}$, Eq. (14) is obtained.

$$\vec{E}_{NC\text{-Total}} = \sum_{i=1}^N(\vec{E}_{NCi} + \vec{E}_{NCi\text{-image}}) \quad (14)$$

A.1.3 Total electric field (\vec{E}_{Total})

The total electric field \vec{E}_{Total} is determined by the vector sum of Eqs. (10) and (14):

$$\vec{E}_{\text{Total}} = \sum_{i=1}^N(\vec{E}_{C\text{-Total}} + \vec{E}_{NC\text{-Total}}) \quad (15)$$

A.2 Potential difference, voltage drop, and step voltage

In several cases, potential difference, voltage drop, and step voltage are more practical parameters. However, these definitions depend on the electric field's nature. For instance, in studying personal protection or electromagnetic compatibility, these parameters may be more interesting and applicable. Here follows a brief definition of each one of them.

A.2.1 Potential difference (Δu) – path independent

The potential difference corresponds to the line integral of $\vec{E}_{C\text{-Total}}$, which depends only on the start (p_1) and end (p_2) points, not depending on the integration path. Thus, it is defined according to Eq. (16).

$$\Delta u = -\int_{p_1}^{p_2}\vec{E}_{C\text{-Total}} \cdot d\vec{\ell} = u_2 - u_1 \quad (16)$$

A.2.2 Voltage drop ($U_{p_1-p_2}$) – path dependent

The voltage drop corresponds to the line integral of \vec{E}_{Total} , which depends on the start and endpoints and the integration path. Thus, it is defined according to Eq. (17).

$$U_{p_1-p_2} = \int_{p_1}^{p_2}\vec{E}_{\text{Total}} \cdot d\vec{\ell} \quad (17)$$

Acknowledgements

This work was financed in part by the Coordenação de Aperfeiçoamento de Pessoal de Nível Superior – Brasil (CAPES), Finance Code 001. It also was partially supported by INERGE (Instituto Nacional de Energia Elétrica), CNPq (Conselho Nacional de Desenvolvimento Científico e Tecnológico), FAPERJ (Fundação Carlos Chagas Filho de Amparo à Pesquisa do Estado do Rio de Janeiro), and FAPEMIG (Fundação de Amparo à Pesquisa do Estado de Minas Gerais).

Author details


Antonio Carlos S. Lima^{1*}, Pedro H.N. Vieira¹, Marco Aurélio O. Schroeder²
and Rodolfo Antônio R. Moura²

1 Federal University of Rio de Janeiro, Rio de Janeiro, Brazil

2 Federal University of São João del-Rei, São João del-Rei, Brazil

*Address all correspondence to: acsl@coppe.ufrj.br

IntechOpen

© 2021 The Author(s). Licensee IntechOpen. This chapter is distributed under the terms of the Creative Commons Attribution License (<http://creativecommons.org/licenses/by/3.0>), which permits unrestricted use, distribution, and reproduction in any medium, provided the original work is properly cited. 

References

- [1] Harrington R. Origin and development of the method of moments for field computation. *IEEE Antennas and Propagation Magazine*. 1990;**32**(3):31-35
- [2] Wedepohl LM, Mohamed SET. Multiconductor transmission lines. Theory of natural modes and Fourier integral applied to transient analysis. *Proceedings of the Institution of Electrical Engineers*. 1969;**116**(9): 1553-1563
- [3] Wilcox DJ. Numerical Laplace transformation and inversion. *International Journal of Electrical Engineering*. 1978;**15**:247-265
- [4] Uribe FA, Naredo JL, Moreno P, Guardado L. Electromagnetic transients in underground transmission systems through the Numerical Laplace Transform. *International Journal of Electrical Power & Energy Systems*. 2002;**24**:215-221
- [5] Moreno P, Ramirez A. Implementation of the Numerical Laplace Transform: A review task force on frequency domain methods for EMT studies. *IEEE Transactions on Power Delivery*. 2008;**23**(4):2599-2609
- [6] Gomez P, Uribe FA. The Numerical Laplace Transform: An accurate technique for analyzing electromagnetic transients on power system devices. *International Journal of Electrical Power & Energy Systems*. 2009;**31**:116-123
- [7] Akbari M, Sheshyekani K, Alemi MR. The effect of frequency dependence of soil electrical parameters on the lightning performance of grounding systems. *IEEE Transactions on Electromagnetic Compatibility*. 2013;**55**(4):739-746
- [8] Grcev L, Dawalibi F. An electromagnetic model for transients in grounding systems. *IEEE Transactions on Power Delivery*. 1990;**5**(4):1773-1781
- [9] Visacro S, Portela CM. Modelling of earthing systems for lightning protection applications, including propagation effects. In: *21st International Conference on Lightning Protection (ICLP)*. Berlin; 1992. pp. 129–132
- [10] Visacro S, Soares A. HEM: A model for simulation of lightning-related engineering problems. *IEEE Transactions on Power Delivery*. 2005; **20**(2):1206-1208
- [11] Tanabe K. Novel method for analyzing dynamic behavior of grounding systems based on the finite-difference time-domain method. *IEEE Power Engineering Review*. 2001;**21**(9): 55-57
- [12] Tsumura M, Baba Y, Nagaoka N, Ametani A. FDTD simulation of a horizontal grounding electrode and modeling of its equivalent circuit. *IEEE Transactions on Electromagnetic Compatibility*. 2006;**48**(4):817-825
- [13] Ruehli AE. Equivalent circuit models for three-dimensional multiconductor systems. *IEEE Transactions on Microwave Theory and Techniques*. 1974;**22**(3): 216-221
- [14] Ruehli A. Partial element equivalent circuit (PEEC) method and its application in the frequency and time domain. In: *Proceedings of Symposium on Electromagnetic Compatibility*. IEEE; 1996. pp: 128–133
- [15] Alipio R, Visacro S. Impulse efficiency of grounding electrodes: Effect of frequency-dependent soil parameters. *IEEE Transactions on Power Delivery*. 2014;**29**(2):716-723
- [16] Sadiku MNO. *Solutions Manual for Numerical Techniques in Electromagnetics*. Florida, US: CRC Press; 1992

- [17] Ho CW, Ruehli A, Brennan P. The modified nodal approach to network analysis. *IEEE Transactions on Circuits and Systems*. 1975;**22**(6):504-509
- [18] Wedepohl L, Jackson L. Modified nodal analysis: An essential addition to electrical circuit theory and analysis. *Engineering Science and Education Journal*. 2002;**11**(3):84-92
- [19] Takashima T, Nakae T, Ishibashi R. Calculation of complex fields in conducting media. *IEEE Transactions on Electrical Insulation*. 1980;**EI-15**(1):1-7
- [20] Takashima T, Nakae T, Ishibashi R. High frequency characteristics of impedances to ground and field distributions of ground electrodes. *IEEE Power Engineering Review*. 1981;**1**(4):60-61
- [21] Arnautovski-Toseva V, Grcev L. On the image model of a buried horizontal wire. *IEEE Transactions on Electromagnetic Compatibility*. 2016;**58**(1):278-286
- [22] Schroeder MAO, Moura RAR, Machado VM. A discussion on practical limits for segmentation procedures of tower-footing grounding modeling for lightning responses. *IEEE Transactions on Electromagnetic Compatibility*. 2020;**62**(2):2520-2527
- [23] Lima ACS, Moura RAR, Vieira PHN, Schroeder MAO, Correia de Barros MT. A computational improvement in grounding systems. Transient analysis. *IEEE Transactions on Electromagnetic Compatibility*. 2020;**62**(3):765-773
- [24] Moura RAR, Schroeder MAO, Lima ACS, Vieira PHN. Closed-form approximation for horizontal grounding electrodes transient analysis. *Journal of Control, Automation and Electrical Systems*. 2020;**31**(4):1063-1073
- [25] Moura RAR, Schroeder MAO, Lima ACS, Vieira PHN, Alipio R. Closed-form approximation for grounding grids transient analysis. *Journal of Control, Automation and Electrical Systems*. 2021;**32**:796-806
- [26] Alipio R, Visacro S. Modeling the frequency dependence of electrical parameters of soil. *IEEE Transactions on Electromagnetic Compatibility*. 2014;**56**(5):1163-1171
- [27] Alipio RS, Schroeder MAO, Afonso MM, Oliveira TAS, Assis SC. Electric fields of grounding electrodes with frequency dependent soil parameters. *Electric Power Systems Research*. 2012;**83**(1):220-226
- [28] Portela CM, Tavares MC, Pissolato FJ. Accurate representation of soil behaviour for transient studies. *IEE Proceedings - Generation, Transmission and Distribution*. 2003;**150**(6):736-744
- [29] Visacro S, Alipio R, Pereira C, Guimarães M, Schroeder MAO. Lightning response of grounding grids: Simulated and experimental results. *IEEE Transactions on Electromagnetic Compatibility*. 2015;**57**(1):121-127